Journal of Alloys and Compounds 509 (2011) 3203–3207

Contents lists available at ScienceDirect

Journal of Alloys and Compounds

journal homepage: www.elsevier.com/locate/jallcom

Synthesis of Li_2MgIr and $LiMgIrH_6$: Guidance from DFT

J.R. Salvador*, J.F. Herbst, M.S. Meyer

Chemical Sciences and Materials Systems Laboratory, General Motors Research and Development Center, 30500 Mound Rd, Mail Code 480-106-224, Warren, MI 48090-9055, United States

ARTICLE INFO

Article history:
Received 11 August 2010
Received in revised form 13 October 2010
Accepted 28 October 2010
Available online 15 December 2010

Keywords:
Hydrogen absorbing materials
Complex hydrides
Electronic band structure
Enthalpy

ABSTRACT

Our theoretical modeling of Li_2MgX systems and their hydrides with density functional theory (DFT) suggested the existence of Li_2MgIr. Verifying the DFT results, we have synthesized Li_2MgIr and determined its crystal structure and hydrogen sorption behavior. The phase crystallizes in the cubic $P\bar{4}3m$ space group and is isostructural to the known ternary Li_2MgSi. Its reaction with hydrogen proceeds according to

$$Li_2MgIr + (7/2)H_2 \rightarrow LiMgIrH_6 + LiH$$

The hydride $LiMgIrH_6$ also features $P\bar{4}3m$ symmetry; its detailed crystal structure is established via a combination of X-ray diffraction and DFT analyses. A metal → insulator transition accompanies formation of the hydride.

1. Introduction

Compounds having the Li_2MgX stoichiometry are known to form for X = Ag, Al, Au, Bi, Cd, Ga, Ge, Hg, In, Pb, Sb, Si, Sn, Tl, and Zn in various cubic space groups [1]. Since such phases contain substantial amounts of the light elements Li and Mg, they merit exploration as potential hydrogen storage media. Using the known structures as templates we have calculated formation enthalpies ΔH via density functional theory (DFT) [2], finding negative values indicating phase formation for the known compounds as well as for other elements X, including Ir and Pt. Here we report formation of the previously unknown ternary intermetallic Li_2MgIr, whose existence was predicted by our DFT calculations, and the determination of its crystal structure. We find that its exposure to hydrogen produces the quaternary hydride $LiMgIrH_6$, also heretofore unknown, whose structure we identify via a combination of X-ray diffraction and DFT work. Li_2MgIr is metallic while the hydride is an insulator.

2. Experimental and computational methods

Li_2MgIr was formed by combining the elements with Li and Ir in their stoichiometric ratios and using a 33% molar excess of Mg to compensate for vapor loss and coating of the reaction vessel. The charge was sealed in a stainless steel tube by arc welding each end, then heating to 510 °C with soaking for 4 days. All sample manipulation was done in an Ar-filled glove box with O_2 and H_2O levels of 2–3 ppm or below. Elemental analysis by inductively coupled plasma mass spectrometry performed on product from the optimized heat treatment with excess Mg indicated Li:Mg:Ir ratios of 2.002:1.05:1, very near the target stoichiometry.

For structural analysis sample powder was loaded into a 1.0 mm quartz capillary and powder X-ray diffraction (PXRD) data collected on a STOE II imaging plate diffractometer with transmission geometry at room temperature with graphite monochromatized Mo K_α radiation. Data were obtained between 5° and 70° 2θ and integrated over the surface of the plate not shadowed by the capillary. The final structure was refined by least squares Rietveld analysis using the FULLPROF suite of programs [3].

Our DFT calculations explored Li_2MgX parent compounds as well as Li_2MgXH_n hydrides of them. The face-centered cubic (fcc) $CuHg_2Ti$-type ($F\bar{4}3m$; space group No. 216) and BiF_3-type ($Fm\bar{3}m$; No. 225) structures, in which many of the known compounds crystallize, were chosen as templates for the parent materials. Eight different template structures were investigated for the XLi_2MgH_n hydrides. Seven of these were generated from the known $PdSr_2LiH_5$ structure (tetragonal $P4mmm$, No. 123) by first making the replacements Pd → X, Sr → Li, and Li → Mg and then introducing 4–6 hydrogen atoms at various sites. The eighth template was derived from the ordered hexagonal ($P6_3mmc$; No. 194) $RuMg_2LiH_7$ structure via the replacements Ru → X, Mg → Li, and Li → Mg. Total electronic energies were computed with the Vienna *ab initio* Simulation Package (VASP), which implements DFT with a plane wave basis set [4,5]. Potentials obtained via the projector-augmented wave approach [6,7] were employed for the elements in conjunction with the generalized gradient approximation of Perdew and Wang [8,9] for the exchange-correlation energy functional. The Li, Mg, Ir, and H potentials contained 3, 8, 9, and 1 valence electrons and were constructed with plane wave energy cutoffs of 272 eV, 266 eV, 211 eV, and 700 eV, respectively. In all self-consistent computations a plane wave cutoff energy of at least 900 eV, much larger than any of the potential cutoffs, was imposed. The k-point spacings of the reciprocal space meshes were no larger than 0.1 $Å^{-1}$. At least two full-cell optimizations of the lattice constants and nuclear coordinates were performed for each material of interest; the total energies were converged to 10^{-6} eV/cell and the forces relaxed to 10^{-4} eV/Å.

3. Crystal structure of Li_2MgIr

Trial structures for analysis of the Li_2MgIr diffraction data included the fcc $Fm\bar{3}m$ and $F\bar{4}3m$ templates [1] employed in our DFT modeling work and the recently reported cubic $P\bar{4}3m$ (space

* Corresponding author. Tel.: +1 586 986 5383; fax: +1 586 986 3091.
E-mail address: james.salvador@gm.com (J.R. Salvador).

0925-8388/$ – see front matter © 2011 Elsevier B.V. All rights reserved.
doi:10.1016/j.jallcom.2010.10.216

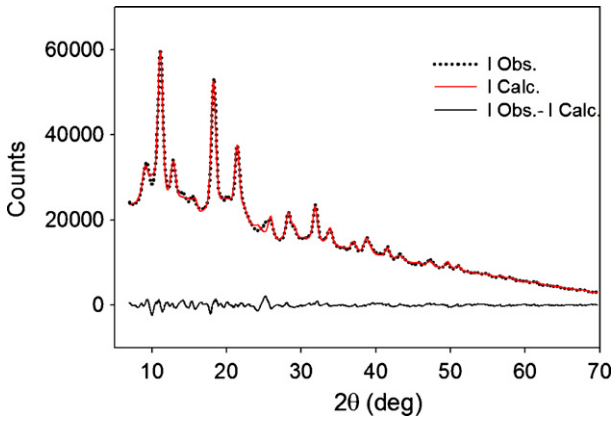

Fig. 1. Powder X-ray Rietveld refinement plot for as-cast Li_2MgIr.

group No. 215) Li_2MgSi structure [10]. One observed low angle reflection in the as-cast Li_2MgIr pattern is forbidden by fcc extinction conditions, while $P\bar{4}3m$ symmetry was found to account for all experimental reflections. The refinement demonstrates that Li_2MgIr and Li_2MgSi are isostructural. Fig. 1 displays the observed and refined diffraction patterns, Fig. 2 is a diagram of the structure, and Table 1 contains the structural information. The Li ions occupy the 1b, 3c and 4e Wyckoff positions, Mg ions are on the 1a and 3d positions, and Ir atoms are located on 4e positions. The Li ions at the 1b and 3c sites and both Mg ions are tetrahedrally coordinated by Ir atoms, while the Li ion on the 4e site resides in a cage and is only loosely bound to surrounding Mg ions. This fact has important implications for the hydriding behavior elaborated in Section 4. The one crystallographically unique Ir site is coordinated with 4 Li and 4 Mg ions in a cuboidal bonding environment. Table 1 also lists the lattice parameters obtained from optimization of the structure with VASP, including the Li 4e site x coordinate which could not be determined accurately from the PXRD data because of the small X-ray scattering cross section of Li. The total energy calculated for the observed $P\bar{4}3m$ structure is E_{el} ($P\bar{4}3m$) = −78.8 kJ mol Li_2MgIr, properly lower than E_{el} ($Fm\bar{3}m$) = −49.9 kJ mol Li_2MgIr

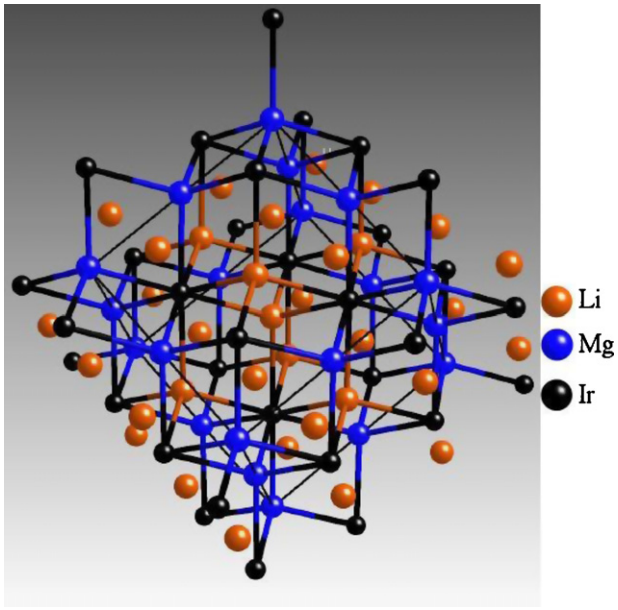

Fig. 2. Crystal structure diagram of Li_2MgIr. The black line indicates the unit cell. All Mg and Li ions with the exception of the 4e Li sites are tetrahedrally coordinated by Ir, and Ir is in an eightfold-coordinated cuboidal environment of 4 Mg and 4 Li ions. The 4e Li ion resides in a cage and is only loosely associated with Mg.

Table 1
Crystallographic information for Li_2MgIr and $LiMgIrH_6$. Both materials form in the cubic $P\bar{4}3m$ space group (No. 215) and have four formula units per unit cell. In Li_2MgIr the Li, Mg, and Ir atoms reside on (1b, 3c, 4e), (1a, 3d), and 4e sites, respectively. In $LiMgIrH_6$ the Li, Mg, Ir, and H positions are (1b, 3c), (1a, 3d), 4e, and ($12i_1$, $12i_2$), respectively.

	Li_2MgIr		$LiMgIrH_6$	
	Observed	DFT	Observed	DFT
a (Å)	6.315(1)	6.206	6.667(1)	6.673
Li 4e x	0.2331	0.2690		
Ir 4e x	0.7511	0.7476	0.7943	0.7575
H $12i_1$ x				0.7508
H $12i_1$ z				0.5081
H $12i_2$ x				0.2514
H $12i_2$ z				0.0072
V (Å^3)	251.8	239.1	296.3	297.2
ρ (g/cm^3)	6.07	6.40	5.15	5.13

and E_{el} ($F\bar{4}3m$) = −76.2 kJ mol Li_2MgIr obtained for the two template structures. Significantly, the $F\bar{4}3m$ template structure, with E_{el} only slightly higher than E_{el} ($P\bar{4}3m$), features a very similar coordination environment for the Li 4d and Mg 4c (Wyckoff positions in the F-centered cell) ions that reside within a tetrahedron of Ir atoms which are themselves inside a cuboidal cage of 4 Li and 4 Mg ions as is the case for the correct primitive cell.

4. Hydriding behavior: formation of $LiMgIrH_6$

Li_2MgIr was successfully hydrided by heating at a rate of 5 °C/min under H_2 at 82 bar to a final temperature of 400 °C. Hydriding of the as-cast sample begins at 180 °C, and the sample had an initial hydrogen uptake of 2.74 mass% corresponding to 6.5 H atoms per Li_2MgIr formula unit. Dehydriding was performed in 1.3 bar of flowing He heated at 5 °C/min to a final temperature of 450 °C. Weight change was monitored as a function of time and temperature.

Analysis of PXRD data revealed the hydride to have the same $P\bar{4}3m$ space group as the Li_2MgIr parent but with a 5% larger lattice parameter. Rietveld refinement found slight shifts in some atomic positions relative to the parent. Though the precise number and location of the lithium and hydrogen atoms could not be obtained from PXRD, we infer that the hydride stoichiometry is $LiMgIrH_6$ for two reasons. First, some of the hydrogen uptake can be attributed to the observed formation of the minor phase Mg_3IrH_5 and to the production of LiH, as we propose below. Second, Ir is known to form $(IrH_6)^{-3}$ complexes with hydrogen, as in Li_3IrH_6 and Na_3IrH_6 [11]. Such configurations obey the "18 electron rule" reflecting closed-shell-type electronic stability. In Li_3IrH_6, for example, Li can be assumed to be Li^{+1}, donating three electrons to the $(IrH_6)^{-3}$ complex which, with 9 electrons from Ir and 6 from hydrogen, thus has a total of 18. $LiMgIrH_6$ also conforms to the rule and based on this a semiconducting/insulating complex hydride is expected. Fig. 3 displays the refinement results.

DFT work also supports the proposed $LiMgIrH_6$ stoichiometry. Calculations for Li_2MgIrH_6 and $LiMgIrH_6$, with hydrogen populating two sets of 12i sites and Li, Mg, and Ir at their positions in Li_2MgIr in the former and the Li 4e site removed from the latter, yielded $E_{el}(Li_2MgIrH_6)$ = −89 kJ mol H_2 and $E_{el}(LiMgIrH_6)$ = −123 kJ mol H_2, so that $LiMgIrH_6$ is clearly preferable energetically. Table 1 includes the VASP-optimized lattice parameters for $LiMgIrH_6$, and Fig. 4 is a diagram of its crystal structure. On the right in Fig. 4 is a view of the $(IrH_6)^{-3}$ anion complex highlighting the octahedral coordination of Ir by H. Not readily apparent is the fact that the Li 4e ions need to be eliminated from the parent structure in order to accommodate the six H atoms, and that elimination enables bond distances similar to those in other Ir hydride systems [11].

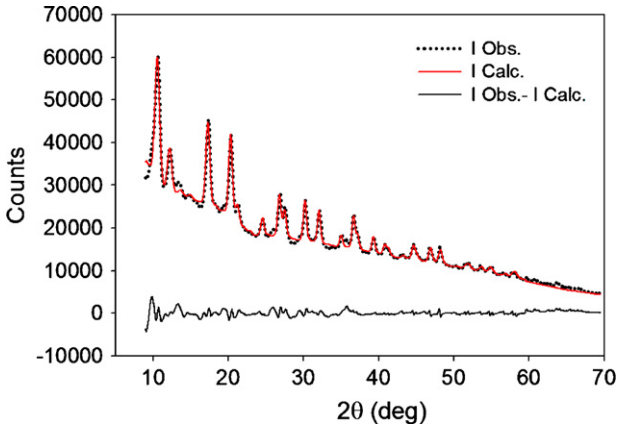

Fig. 3. Powder X-ray Rietveld refinement plot for the hydride $LiMgIrH_6$.

Given the $LiMgIrH_6$ hydride stoichiometry and the previous observation that the Li 4e ions are only loosely coordinated in the Li_2MgIr parent lattice, and so are most likely prone to migration under appropriate conditions, we propose that the hydriding reaction is

$$Li_2MgIr + (7/2)H_2 \rightarrow LiMgIrH_6 + LiH \quad (1)$$

This accounts well for the initial hydrogen uptake, and the stoichiometry is consistent with the multiplicity of the Li 4e site, which we infer to diffuse out of Li_2MgIr to form LiH on hydriding. Further substantiating the hydriding scheme were results of density measurements of the hydrided products that found that its density agrees well with that predicted for a 1:1 molar ratio mixture of $LiMgIrH_6$ and LiH. It is significant to note that the isostructural compound Li_2MgSi is also destabilized by reacting with hydrogen at elevated temperature, completely delithiating to form Mg_2Si, Si, and LiH [10]. Further underscoring Li_2MgIr's propensity for delithiation is the fact that if stored under a N_2 atmosphere this compound will decompose to form Li_3N at room temperature over the course of a week.

While the Li_2MgIr sample was a loose gray powder, inspection of the hydriding product found it to have considerably finer grains and an olive green hue indicating the formation of a semiconducting/insulating product; it also transmitted mid-range infrared radiation. The DFT calculations reveal a metal–insulator transition as well, consistent with the closed shell electronic configuration

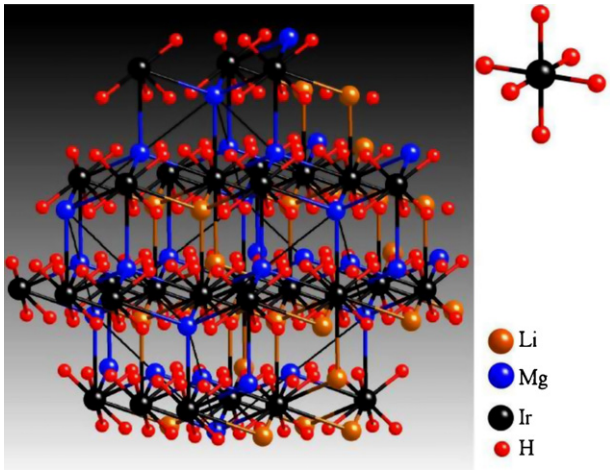

Fig. 4. Proposed crystal structure of $LiMgIrH_6$. Atomic coordinates taken from the VASP relaxed structure. Figure on the right shows the octahedral coordination environment of Ir by H in the $(IrH_6)^{-3}$ ionic complex.

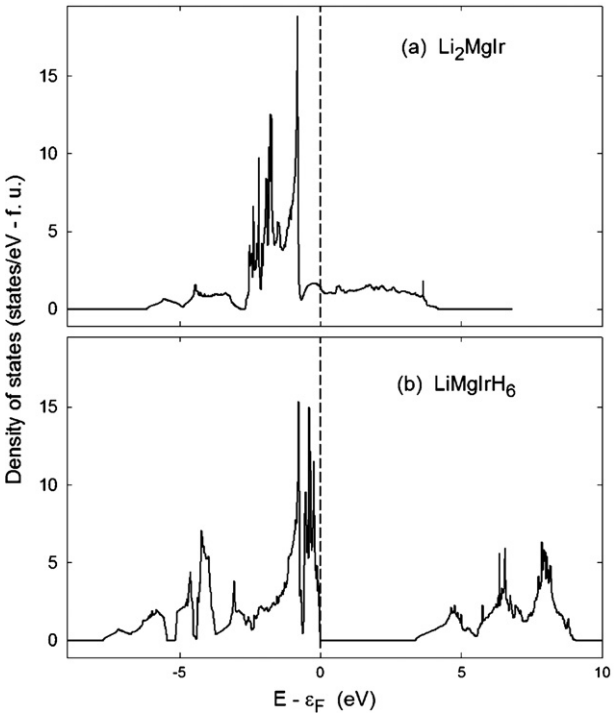

Fig. 5. Calculated electronic density of states vs. energy with respect to the Fermi level ε_F for (a) Li_2MgIr and (b) $LiMgIrH_6$.

of the hydride explained above. Fig. 5(a) shows the total density of states (DOS) calculated for the Li_2MgIr parent material. Immediately obvious is the presence of significant electron density at the Fermi level ε_F, indicating a metallic compound. This was supported experimentally by finding that Li_2MgIr was opaque to mid-range infrared radiation. Examination of the atom resolved, orbitally decomposed DOS (Fig. 6(a)–(c)) shows that the frontier orbitals (states at and near ε_F) are populated by the *s* and *p* bands of Li and Mg as well as the 5*d* bands of Ir. In fact, the Ir 5*d* bands make the largest contribution to the DOS at the Fermi level. This indicates strong hybridization of the Li and Mg *s* and *p* states with the Ir *d* states in the parent compound. Furthermore, the fact that the *d* states of Ir play a dominant role in the frontier orbitals makes them available for overlap and bond formation during the hydriding reaction. The total DOS computed for $LiMgIrH_6$, displayed in Fig. 5(b), confirms this point since the Ir 5*d* bands clearly dominate in the energy range just below ε_F. Additionally, the 3.4 eV gap above ε_F demonstrates that the hydride is an insulator, in qualitative agreement with our observations. The calculated band structure of $LiMgIrH_6$ in Fig. 7 shows that the band gap is indirect: while the conduction band minimum is at the Γ point in the Brillouin zone, the valence band maximum is located between the Γ and M points.

Although the DFT exploratory effort suggested the possible formation of a Li_2MgIrH_n hydride for each of the eight templates, the $LiMgIrH_6$ phase we have actually synthesized has a structure distinct from all the templates as well as a different stoichiometry. This illustrates the important point that model calculations, however encouraging, can only be considered as guides for the identification of new materials. Complementary experimental investigation is absolutely essential. In the present case we calculate the standard enthalpy of formation (at 0 K and without the zero point energy)

$$\begin{aligned}\Delta H(LiMgIrH_6) &= E_{el}(LiMgIrH_6) - E_{el}(Li) - E_{el}(Mg) \\ &\quad - E_{el}(Ir) - 3E_{el}(H_2) \\ &= -122\ \text{kJ/mol H}_2\end{aligned} \quad (2)$$

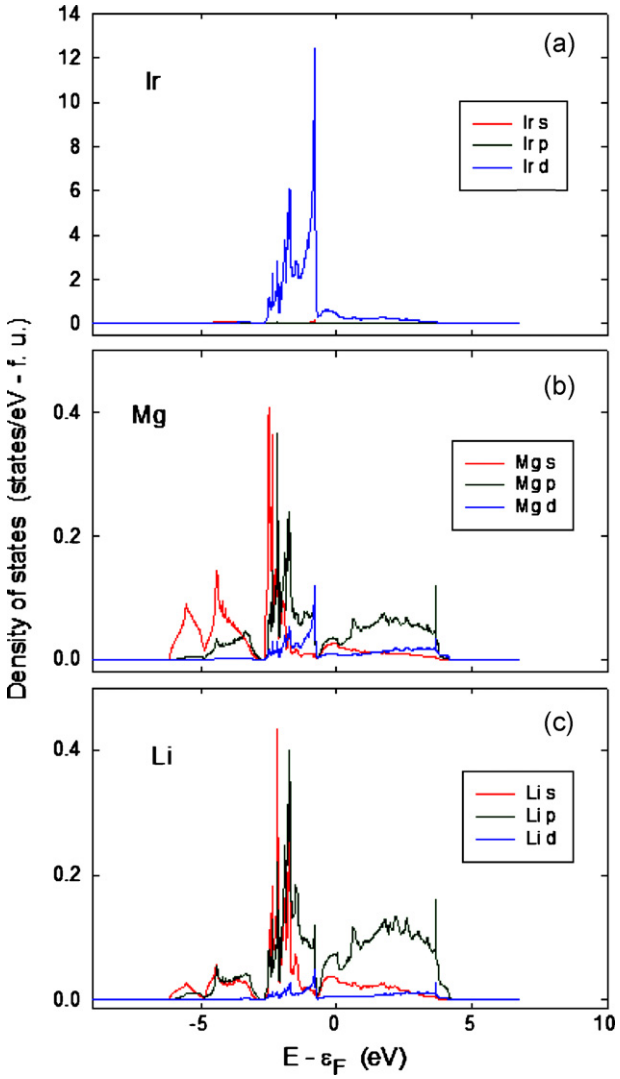

Fig. 6. Atom resolved, orbitally decomposed densities of states calculated for Li_2MgIr: (a) Ir, (b) Mg, and (c) Li.

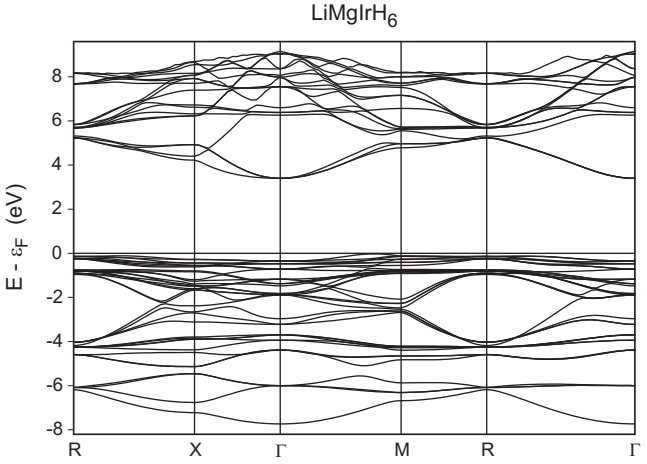

Fig. 7. Band structure calculated for $LiMgIrH_6$.

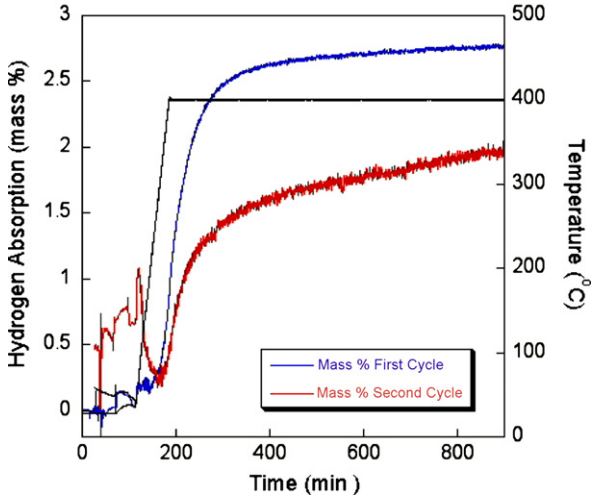

Fig. 8. Thermal absorption curves for the first (blue) and second (red) cycle of hydrogen uptake for Li_2MgIr. The black line indicates the temperature profile as a function of time for the thermal absorption experiment. (For interpretation of the references to color in this figure legend, the reader is referred to the web version of the article.)

for the new hydride. Significantly, this value is lower than for any of the eight template hydride structures. Once the true crystal structure is identified, DFT will almost invariably demonstrate it to have an energy lower than that of any alternatives. For the enthalpy of reaction (1) we find

$$\begin{aligned}\Delta H_R &= \Delta H(LiMgIrH_6) + \Delta H(LiH) - \Delta H(Li_2MgIr)\\ &= E_{el}(LiMgIrH_6) + E_{el}(LiH) - E_{el}(Li_2MgIr) - (7/2)E_{el}(H_2)\\ &= -124\,kJ/mol\ H_2,\end{aligned} \tag{3}$$

so that the $LiMgIrH_6$ and LiH hydriding products are very stable with respect to the reactants.

To establish if reaction (1) could be cycled repeatedly the original as-cast Li_2MgIr was hydrided to the cubic complex hydride and LiH, then thermally desorbed by ramping to 450 °C; only 2.0 mass% was liberated or approximately 5 hydrogen atoms per formula unit. The PXRD pattern of the dehydrided product contained two broad, featureless peaks, obviating identification of the components. Upon rehydriding this nearly amorphous sample, the cubic complex hydride was recovered as confirmed by PXRD. This process was repeated several times, but with each additional cycle the amount of absorbed hydrogen decreased and the amount of thermally desorbed hydrogen also diminished. Fig. 8 shows the hydrogen uptake of the first and second thermal hydriding cycles demonstrating the reduction of gravimetric capacity with cycling. We conclude that the Li_2MgIr parent phase cannot be recovered after hydride formation due to the fact that the temperature required to liberate Li from the LiH product phase exceeds the stability range of Li_2MgIr. Differential scanning calorimetry of the elements and of as-cast Li_2MgIr found an exothermic response at 550 °C and subsequent PXRD found the material to be a mixture of LiIr and MgIr binary phases indicating decomposition above this temperature. LiH, in the absence of any destabilizing materials, decomposes above 800 °C, well above the decomposition temperature of the parent Li_2MgIr. The likely reason for the deterioration in hydrogen capacity of this system is the fact that upon dehydriding a mixture of binary and possibly elemental components results that upon rehydriding may form hydrides themselves, thereby depleting the reactant reservoir required to reform the cubic complex hydride. Continued cycling progressively degrades the system, slowly diluting the cubic complex hydride with other phases that do not release hydrogen unless heated to temperatures higher than those used for

this investigation. Therefore, this material system does not cycle hydrogen reversibly.

5. Summary and conclusions

We have synthesized the previously unknown ternary intermetallic, Li_2MgIr, whose formation was suggested by our DFT work. The phase crystallizes in the primitive cubic $P\bar{4}3m$ space group and is isostructural with Li_2MgSi. It reacts with H_2 to form LiH and a new Li–Mg–Ir hydride. Analysis of powder X-ray diffraction data, hydrogen uptake measurements, electron counting rules, and DFT studies suggest that the hydride stoichiometry is $LiMgIrH_6$ with the inference that the Li 4e site ions diffuse out of Li_2MgIr to form LiH on exposure to H_2. In concert with DFT the $LiMgIrH_6$ crystal structure was determined to be isomorphic with the parent compound. $LiMgIrH_6$ is insulating, so that a metal → insulator transition accompanies the hydriding reaction, which we identify as

$$Li_2MgIr + (7/2)H_2 \rightarrow LiMgIrH_6 + LiH$$

Due to the high hydrogen release temperature of LiH and the fact that Li_2MgIr decomposes at temperatures above 550 °C, the parent phase cannot be recovered from the hydride under any desorption conditions we employed. The system will absorb and desorb hydrogen repeatedly, forming the cubic complex hydride but without recovery of Li_2MgIr. Even ignoring the fact that Ir is a precious metal, the slow build-up of secondary phases with hydrogen cycling gradually deteriorates the hydrogen capacity of the system, making it unsuitable for hydrogen storage applications.

Acknowledgements

It is a pleasure to thank Richard L. Speer for powder X-ray diffraction, Nick Irish for ICPMS elemental analysis and Deborah Eckel for FTIR analysis. Mercouri G. Kanatzidis and the diffraction facility at Northwestern University for use of the STOE II X-ray diffractometer are also gratefully acknowledged.

References

[1] P. Villars, L.D. Calvert, Pearson's Handbook of Crystallographic Data for Intermetallic Phases, 2nd ed., ASM International, Materials Park, OH, 1991.
[2] W. Kohn, L. Sham, Phys. Rev. 140 (1965) A1133.
[3] J. Rodríguez-Carvajal, Presented at the Satellite Meeting on Powder Diffraction of the XV IUCr Congress, 1990, p. 127.
[4] G. Kresse, J. Hafner, Phys. Rev. B 49 (1994) 14251.
[5] G. Kresse, J. Furthmüller, Comput. Mater. Sci. 6 (1996) 15.
[6] P.E. Blöchl, Phys. Rev. B 50 (1994) 17953.
[7] G. Kresse, D. Joubert, Phys. Rev. B 59 (1999) 1758.
[8] J.P. Perdew, Y. Wang, Phys. Rev. B 45 (1992) 13244.
[9] J.P. Perdew, J.A. Chevary, S.H. Vosko, K.A. Jackson, M.R. Pederson, D.J. Singh, C. Fiolhais, Phys. Rev. B 46 (1992) 6671.
[10] J.F. Herbst, M.S. Meyer, J. Alloys Compd. 492 (2010) 65.
[11] K. Yvon, Encyclopedia of Inorganic Chemistry, vol. 3, Wiley, Chichester, 1994, p. 1418.